142

A. Vejdani-Noghreiyan, *et al.*: Theoretical and Experimental Determination of ...
Nuclear Technology & Radiation Protection: Year 2016, Vol. 31, No. 2, pp. 142-149

# THEORETICAL AND EXPERIMENTAL DETERMINATION OF MASS ATTENUATION COEFFICIENTS OF LEAD-BASED CERAMICS AND THEIR COMPARISON WITH SIMULATION

by

## Alireza VEJDANI-NOGHREIYAN [1*], Elham ALIAKBARI [1], Atiyeh EBRAHIMI-KHANKOOK [1], and Mahdi GHASEMIFARD [2]

[1] Physics Department, Faculty of Sciences, University of Neyshabur, Neyshabur, Iran
[2] Nanotechnology Laboratory, Esfarayen University of Technology, Esfarayen, Iran

Mass attenuation coefficient of lead-based ceramics have been measured by experimental methods and compared with theoretical and Monte Carlo simulation results. Lead-based ceramics were prepared using mixed oxide method and the X-ray diffraction analysis was done to evaluate the crystal structure of the produced handmade ceramics. The experimental results show good agreement with theoretical and simulation results. However at two gamma ray energies, small differences between experimental and theoretical results have been observed. By adding other additives to ceramics and observing the changes in the shielding properties such as flexibility, one can synthesize and optimize ceramics as a neutron shield.

*Key words: attenuation coefficient, CsI(Tl) detector, lead-based ceramic, MCNP-4C*

## INTRODUCTION

Nowadays ionizing radiation is widely used for medical and industrial applications. The harmful effects of incident radiation on living tissues of human body elevate the risk of cancer. Therefore, it is essential to protect people against the radiation exposure by using suitable shielding materials [1, 2]. The ability of shielding materials in reducing the intensity of radiation is expressed by linear and mass attenuation coefficients.

Ceramic materials are widely used in medicine, aerospace and construction industries. Ceramics are used today as femoral heads and acetabular cups for total hip replacement, dental implants and restorations, bone fillers and scaffolds for tissue engineering [3-5]. Some of ceramics are used as electrolytes for solid oxide fuel cells [6]. They can also be used as radiation shielding for gamma rays. High melting temperature, high chemical resistance in acidic or caustic environments and high hardness are some of the typical properties of ceramics which make them essential for our daily lifestyle [7, 8]. High melting temperature, high heat resistance and high chemical resistance are the advantages of ceramics in comparison with metals and make them suitable for using as radiation shielding material in various environments and different places, especially when using metals is unsuitable. In 2004, Krasnyi *et al.*, studied the chemical resistance of ceramic materials in acids and alkalis and showed that corundum ceramics and mullite ceramics have high values of acid and alkali resistance [9]. Moreover, She and Ohji have studied the characteristics of high porous mullite ceramics and have shown that as the sintering temperature increases from 1450 to 1650 °C the flexural strength increases and a relatively high surface area is achieved which makes porous mullite ceramics suitable for high-temperature catalysis applications as catalyst supports [10].

In this paper, the capability of using different lead-based ceramics as the gamma shield has been studied.

To compare the gamma ray shielding ability of different materials, a mass attenuation coefficient ($\mu/\rho$) is introduced. This parameter describes the probability of all possible interactions between incident photons and matter in unit mass per unit area. Determination of the accurate value of mass attenuation coefficient is important and essential in many applied fields such as nuclear physics and radiation dosimetry [11].

The mass attenuation cofficient depends on the incident gamma ray energy, the effective atomic number of the material ($Z_{eff}$) and the density of the shielding material [12-15]. High atomic number materials such as lead have high attenuation coefficients and are good candidates to be used as the radiation shield [16, 17].

*Corresponding author; e-mail: vejdani_ir@yahoo.com,
vejdani@neyshabur.ac.ir

Several experimental and theoretical works were performed on evaluating the mass attenuation coefficients of different materials with specific applications such as concretes, semi-conductors, some types of polymers, alloys and steels [18-24].

In this study, some lead-based ceramics have been prepared with the purpose of measuring the radiation shielding parameters. The attenuation coefficients of prepared ceramics were measured using the standard gamma sources such as $^{137}$Cs, $^{22}$Na, and $^{60}$Co. Finally, measured results were compared with the results obtained by Monte Carlo simulation and those calculated using the exisiting library data.

## THEORY

When a gamma ray passes through the matter, the variation of gamma ray intensity against thickness of the absorber material is given by the Beer Lambert law

$$I = I_0 \exp(-\mu x) \qquad (1)$$

where $I_0$ is the number of particles of radiation counted during a certain time duration without any absorber, $I$ – the number of counted radiation during the same time, which passes through an absorber (located between the radiation source and the detector) with a thickness of $x$, and $\mu$ – the linear attenuation coefficient of the absorber. The linear attenuation coefficient ($\mu$) shows the probability of photon interaction per unit path length of incident photon when it passes through the matter. It depends on the density of medium which photon passes through. A more useful parameter which is independent of the density of the medium is called mass attenuation coefficient ($\mu_m$). It is the ratio of $\mu/\rho$ that shows the average number of photon interactions in the medium of unit mass per unit area [25]

$$\frac{\mu}{\rho} = \frac{\ln \dfrac{I_0}{I}}{\rho x} \qquad (2)$$

where $\rho$ is the density of material [kgm$^{-3}$]. The accurate value of mass attenuation coefficient is essential to obtain shielding and dosimetric parameters used in many applied fields such as radiation protection and radiation dosimetry. In addition, the total mass attenuation coefficient $(\mu/\rho)_C$ for any chemical compound or mixture of elements is given by mixture rule [26]

$$\frac{\mu}{\rho}\bigg|_{compound} = \sum_i w_i \frac{\mu}{\rho}\bigg|_i \qquad (3)$$

in which $w_i$ is the weighting fraction of each element in mixture and $(\mu/\rho)_i$ – the mass attenuation coefficient of the $i^{th}$ constituent element. For a chemical compound, the weight fraction is given by

$$w_i = \frac{a_i A_i}{\sum_j a_j A_j} \qquad (4)$$

where $A_i$ is the atomic weight of the $i^{th}$ element and $a_i$ is the number of the element in the related chemical formula of the compound. In this work, considering attenuation coefficient of each element, which is available in nuclear data libraries, the theoretical value of the mass attenuation coefficient for a mixture or compound was computed using a FORTRAN program. This program is based on the mixture rule to calculate the partial and total mass attenuation coefficients for all elements, compounds and mixtures at standard as well as selected energies.

## EXPERIMENTAL

### Production of ceramic samples

In this research, the mixed oxide method has been used for preparing powders of ceramics with formula $(Pb_{0.9}Ba_{0.1})AO_3$, in which the elements Mg, Zn, Cu, Fe, and Mn are denoted by A. Samples were made disc-shaped, of 0.025 m in diameter with thicknesses ranging from 0.002 to 0.006 m [27, 28]. Table 1 shows the elemental composition used to make 0.04 kg of different ceramics investigated in this study. The density of each sample was measured by archimedes principle using water as the immersion fluid. Figure 1 shows 0.002 m-thick handmade samples of different types of ceramics investigated in this work.

### X-ray diffraction analysis and phase evaluation

The phase evolutions and crystal structure of the ceramic powders were studied by X-ray diffraction (XRD, Model Philips X'pert, Cu Ka radiation). Figure 2 shows the XRD patterns of $(Pb_{0.9}Ba_{0.1})MgO_3$ and

**Table 1. Values of chemical compositions ($10^{-3}$ kg) for 0.04 kg of ceramic samples**

| Composition | Ceramics | | | | |
|---|---|---|---|---|---|
| | $(Pb_{0.9}, Ba_{0.1})ZnO_3$ | $(Pb_{0.9}, Ba_{0.1})FeO_3$ | $(Pb_{0.9}, Ba_{0.1})MgO_3$ | $(Pb_{0.9}, Ba_{0.1})CuO_3$ | $(Pb_{0.9}, Ba_{0.1})MnO_3$ |
| PbO | 25.62 | 26.42 | 29.48 | 25.76 | 26.5 |
| Ba(NO)$_3$ | 3.32 | 3.42 | 3.82 | 3.34 | 3.42 |
| Mg(NO)$_3$ | – | – | 37.62 | – | – |
| Fe(NO)$_3$ | – | 53.14 | – | – | – |
| CuSO$_4$ | – | – | – | 20.46 | – |
| ZnO | 10.38 | – | – | – | – |
| MnO$_2$ | – | – | – | – | 11.46 |

144

A. Vejdani-Noghreiyan, *et al.*: Theoretical and Experimental Determination of ...
Nuclear Technology & Radiation Protection: Year 2016, Vol. 31, No. 2, pp. 142-149

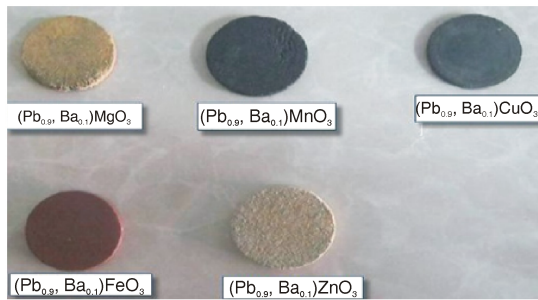**Figure 1. Disks samples of all ceramics**
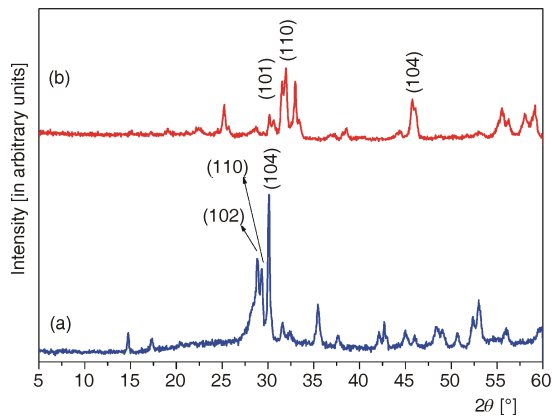


**Figure 2. The XRD pattern of the ceramic prepared at 700 °C; (a) (Pb$_{0.9}$ Ba$_{0.1}$)MgO$_3$, (b) (Pb$_{0.9}$ Ba$_{0.1}$)FeO$_3$**



**Figure 3. SEM images of the surface and particle size distributions of the ceramics; (a, b) (Pb$_{0.9}$ Ba$_{0.1}$)CuO$_3$, (c, d) (Pb$_{0.9}$ Ba$_{0.1}$)ZnO$_3$**
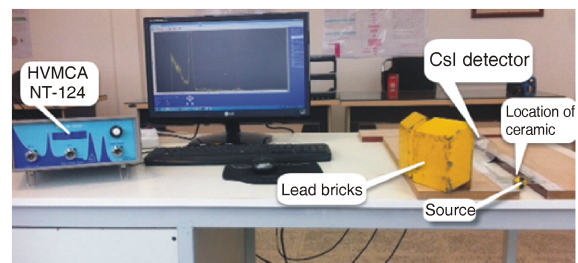


**Figure 4. Photograph of experimental set-up**

(Pb$_{0.9}$Ba$_{0.1}$)FeO$_3$ ceramics. The XRD results reveal the existence of a phase with tetragonal structure for ceramic prepared by the mixed oxide method. The results were summarized in tab. 2.

## SEM image analysis

A typical microstructure of (Pb$_{0.9}$Ba$_{0.1}$)CuO$_3$ and (Pb$_{0.9}$Ba$_{0.1}$)ZnO$_3$ are determined by scanning electron microscopy (SEM) images. The SEM images surface and histogram graphs of samples are shown in fig. 3. According to the fig. 3(a) and fig. 3(c),the shapes of the most particles were found polyhedral.

## Measurement of mass attenuation coefficients

Figure 4 shows the experimental setup used in the present work. Measuring the gamma-ray attenuation coefficient was performed using CsI (Tl) scintillation de-
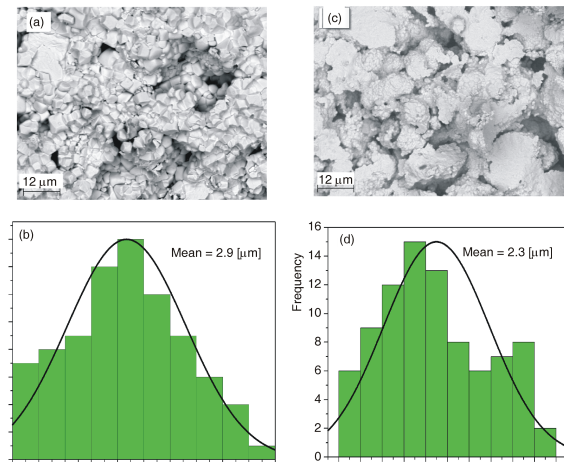
tector with the dimensions of 2"×2" and energy resolution of 6.91% (662 keV) and 5.06% (1173 keV).The detector was connected to the scintillation counter with multi-channel analyzer (MCA) facility, which was connected to an advanced computer system. As aforementioned three radioactive gamma sources including $^{60}$Co, $^{137}$Cs, and $^{22}$Na were used. The spectrometer has been calibrated using gamma rays with energies of 662 keV of $^{137}$Cs source and 1173, and 1332 keV of $^{60}$Co source. Ceramic samples were placed individually between the gamma ray source and the detector. The distances of radioactive source and detector window from the sample were 0.001 and 0.3 m, respectively. The experimental set-up was arranged in such a way that gamma rays passing directly through the sample without any interaction have the greatest chance of achieving the detector. Actually, the relatively large distance between the sample and detector causes that photons which interacted within the

**Table 2. The structure parameters of ceramic powders calcined at 700 °C**

| Ceramics | $2\theta$ | hkl | Structure | Lattice parameter [nm] | Volume of cell [nm$^3$] |
|---|---|---|---|---|---|
| (Pb$_{0.9}$, Ba$_{0.1}$)MgO$_3$ | 28/835 | 102 | Tetragonal | $a = b = 3/96$ | 182/079 |
| | 29/345 | 110 | P4/nmm | $c = 11/611$ | |
| | 30/105 | 104 | | | |
| (Pb$_{0.9}$, Ba$_{0.1}$)FeO$_3$ | 29/190 | 101 | Tetragonal | $a = b = 4/52$ | 235/97 |
| | 32/475 | 110 | P4/nmm | $c = 11/550$ | |
| | 46/560 | 104 | | | |

sample and deviated from the initial beam, cannot reach the detector.

For each evaluation, the spectra were obtained for a period of 600 seconds with varying thickness of ceramic sample. The same process was carried out for all of samples. The numbers of counts reaching the detector with and without the samples under study were recorded. For evaluating the energy peaks of each energy beam, the area underneath the peaks (number of counts) was integrated.

In order to determine $I$ and $I_0$, the net area under the photopeak was taken into account. Considering $I$ and $I_0$ as the measured count rates in detector with and without the absorber with thickness of $x$, respectively, the linear attenuation coefficient can be extracted from the graph, which indicates the linear dependency of the logarithm of ($I_0/I$) on the ceramic thickness. Observed points were seen to be closely distributed around the line, having positive slope. This line was assessed by fitting the experimental data by the least square method. The line slope was used to determine the linear attenuation coefficient. The mass attenuation coefficient was also obtained by dividing the linear attenuation coefficient of the samples by their densities.

## SIMULATION

Computer codes based on the Monte Carlo method were used for calculating mass attenuation coefficients of different types of concrete, heavy metal oxide glasses and polymers [12, 29-32]. In the present study, Monte Carlo N-Particle transport code (MCNP-4C) developed by Los Alamos National Laboratory has been used to perform the simulations. MCNP is a general multipurposes code which can be used effectively to calculate mass attenuation coefficients of different types of mixtures and also has a wide range of capabilities which makes it useful for medical and industrial purposes [33-37]. The Monte Carlo method is based on generating random numbers to simulate any problem having probabilistic interpretation such as photon transport through the matter. In the method, the rules of photon transport are used to create probability distributions. The code uses cross-section libraries to produce probility distributions based on the physical rules of photon transport. The step size of photon interaction between two interaction and type of photon interaction that may occur are produced by using random numbers generated by the appropriate probability distributions. Due to the statistical nature of the Monte Carlo method, a large number of particles should be tracked to obtain reasonable final results.

In this work, the geometry shown in fig. 5 was simulated using MCNP-4C code. As it can be seen in this figure, the ceramic sample shown as a disk was simulated between the point isotropic gamma source
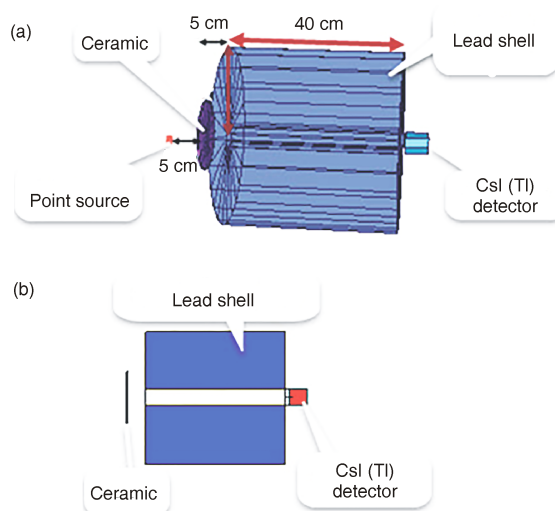


**Figure 5. The assumed geometry simulated by MCNP code; (a) three-dimensional, (b) two-dimensional**

and CsI scintilation detector. Cylinderical shell of lead with inner diameter of 2 inch and outer diameter of 16 inch was simulated between the sample and detector. The number of radiations reached to the detector without any interaction was determined by calculating F1 tally on the detector surface. The attenuation coefficient can be obtained by inserting the assessed results into eq. (1).

## RESULTS AND DISCUSSION

Mass and linear attenuation coefficients of different lead-based ceramics have been investigated experimentally using standard gamma sources. Figure 6 shows the linear dependency of $\mathrm{Ln}(I/I_0)$ *vs.* the thickness of $(Pb_{0.9}Ba_{0.1})ZnO_3$ ceramic for different gamma ray energies. In this figure the slope of the fitted line shows the linear attenuation cofficient ($\mu$). The same procedure was carried out to obtain the value of linear attenuation coefficient for other ceramics as well.

Table 3 shows the resulting values of mass attenuation coefficient ($\mu/\rho$) at different energies, using experimental, theoretical and simulation methods. As it can be seen in this table the experimental results are in good agreement with theoretical and simulation results.

It is seen that there are differences of about 1-9%, and up to 20% in the $ZnO_2$ case, between experimental and simulation results at photon energies 1173 and 1332 keV. The same differences between the experimental and simulation results have been observed in several studies previously [38-40]. The results reported by Icelli *et al.* show differences of about 7-26 % for simple compounds and much greater differences for complex compounds [40]. In addition, a study performed by Sogut *et al.* shows that the total mass attenuation coefficient values of Fe and Cu in the chemical form are dif-
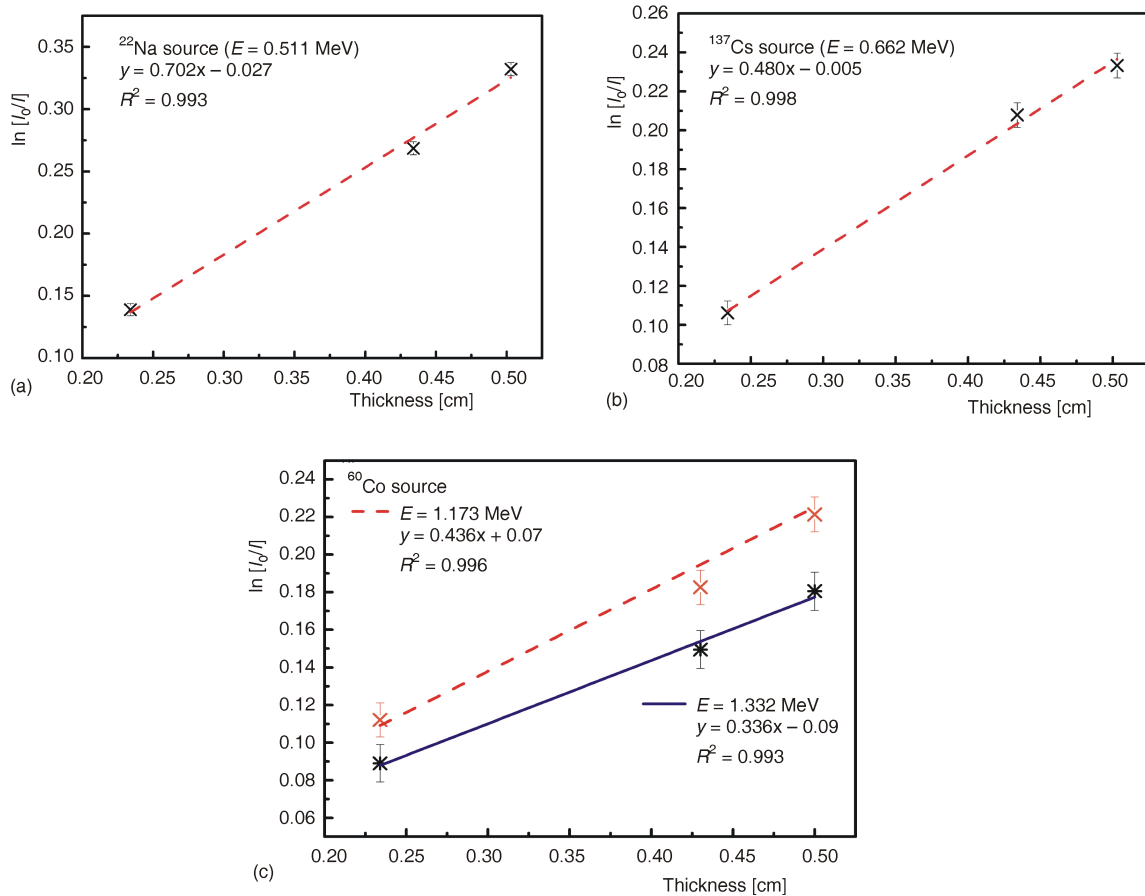
146

A. Vejdani-Noghreiyan, *et al.*: Theoretical and Experimental Determination of  ...
Nuclear Technology & Radiation Protection: Year 2016, Vol. 31, No. 2, pp. 142-149

Figure 6. Plot of $\ln(I_0/I)$ *vs.* thickness $x$ for ceramic $(Pb_{0.9}Ba_{0.1})ZnO_3$ using (a) $^{22}Na$, (b) $^{137}Cs$, and (c) $^{60}Co$ sources

**Table 3. Theoretical, simulations and experimental values of mass attenuation coefficients $\mu/\rho$ ($10^{-1}m^2kg^{-1}$) for all of the ceramic samples**

| Energy [keV] | Method | Ceramics | | | | |
|---|---|---|---|---|---|---|
| | | $(Pb_{0.9}Ba_{0.1})ZnO_3$ ($\rho = 5.72$) | $(Pb_{0.9}Ba_{0.1})FeO_3$ ($\rho = 5.95$) | $(Pb_{0.9}Ba_{0.1})MgO_3$ ($\rho = 6.22$) | $(Pb_{0.9}Ba_{0.1})CuO_3$ ($\rho = 5.12$) | $(Pb_{0.9}Ba_{0.1})MnO_3$ ($\rho = 5.62$) |
| 511 | Theo. | 0.121 | 0.092 | 0.093 | 0.121 | 0.091 |
| | Sim. | 0.119   0.001 | 0.110   0.001 | 0.107   0.001 | 0.123   0.001 | 0.107   0.001 |
| | Exp. | 0.123   0.001 | 0.104   0.0007 | 0.101   0.0008 | 0.118   0.0011 | 0.102   0.0008 |
| 662 | Theo. | 0.093 | 0.076 | 0.077 | 0.094 | 0.076 |
| | Sim. | 0.083   0.001 | 0.077   0.001 | 0.076   0.001 | 0.089   0.001 | 0.076   0.001 |
| | Exp. | 0.084   0.001 | 0.077   0.001 | 0.072   0.001 | 0.089   0.001 | 0.075   0.001 |
| 1173 | Theo. | 0.059 | 0.054 | 0.054 | 0.058 | 0.054 |
| | Sim. | 0.065   0.002 | 0.053   0.002 | 0.051   0.009 | 0.054   0.007 | 0.049   0.004 |
| | Exp. | 0.076   0.002 | 0.057   0.002 | 0.054   0.001 | 0.056   0.002 | 0.054   0.002 |
| 1332 | Theo. | 0.054 | 0.050 | 0.050 | 0.053 | 0.050 |
| | Sim. | 0.054   0.004 | 0.052   0.003 | 0.050   0.003 | 0.052   0.004 | 0.050   0.001 |
| | Exp. | 0.058   0.002 | 0.052   0.002 | 0.049   0.002 | 0.048   0.002 | 0.047   0.002 |

ferent from that of pure elements by 6-17 % [38]. Therefore, it is seen that in comparison with similar studies, the differences between our theoretical and experimental results seems to be in acceptable range. The differences are due to the individual characteristics of structure of molecules, molecular bonding and chemical effects of compounds, which are not considered in theoretical method of calculating mass attenuation coefficient by mixture rule [38, 40].

Regardless of observed differences between theory, simulation and experiment, measured values of mass attenuation coefficients for different ceramics are close to each other. This is because ceramics have similar structural components contained Pb and Ba which play main role in determining attenuation coefficient. However, slight discrepancies between attenuation coefficients of different ceramics are due to differences in one component of ceramics. As it is seen in
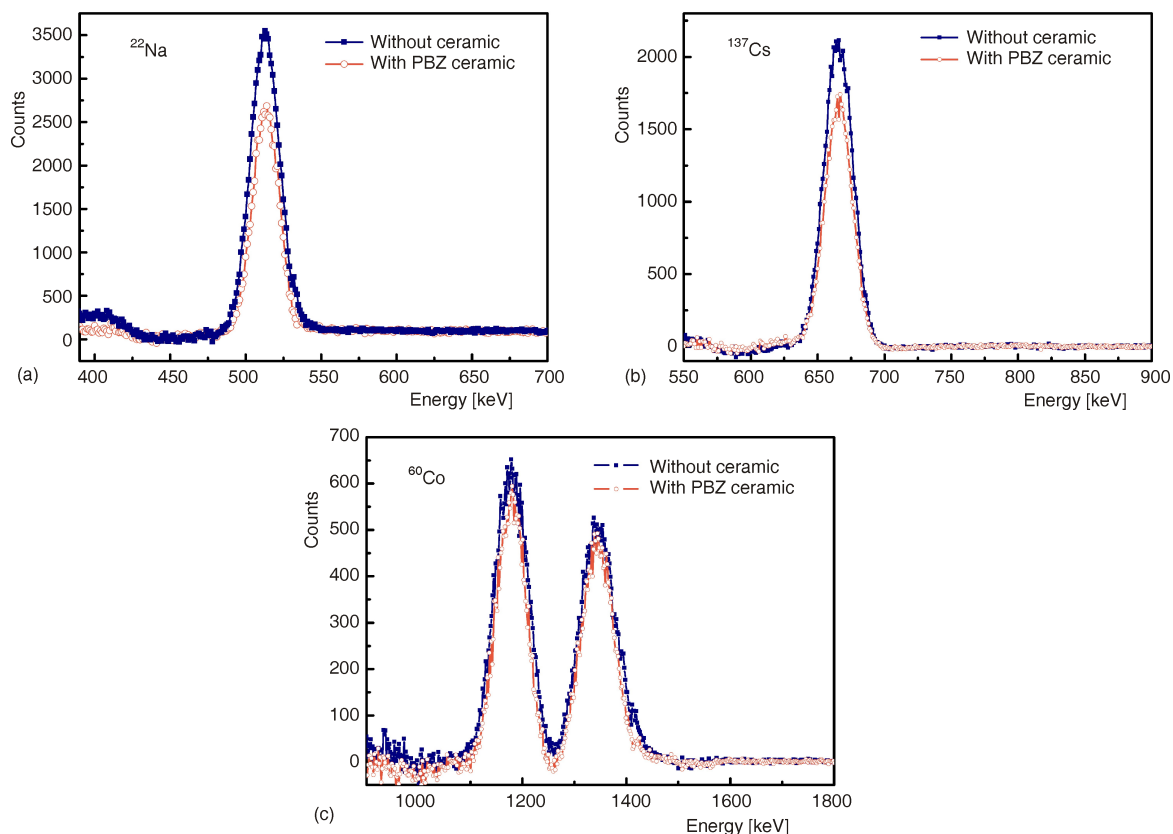
**Figure 7. Spectrum of gamma-rays of sources without attenuation and attenuated by ceramics (Pb$_{0.9}$ Ba$_{0.1}$)ZnO$_3$ with thikness of 5 mm; (a) $^{22}$Na source (b) $^{137}$Cs source, and (c) $^{60}$Co source**

tab. 3, ceramics containing Zn and Cu have higher attenuation coefficient values and ceramics which contain Mg, Mn, and Fe have lower attenuation coefficients. It can be explained by the strong influence of atomic number of the medium on the relative probabilities of photon interactions [41].

It is also obvious from tab. 3 that the mass attenuation coefficients strongly depend on the photon energy. By increasing the photon energy, the mass attenuation coefficients of the investigated compounds are reduced. Figure 7 shows attenuated spectrum of different gamma sources in the presence of (Pb$_{0.9}$Ba$_{0.1}$)ZnO$_3$ ceramic in comparison with the non-attenuated spectrum. It can be seen that for cobalt source, which has higher energy photons than cesium and sodium, the attenuation power of ceramic is small. This finding is in compliance with the fact that the probability of photon interaction with matter decreases by increasing photon energy.

According to tab. 3, (Pb$_{0.9}$Ba$_{0.1}$)ZnO$_3$ and (Pb$_{0.9}$Ba$_{0.1}$)MgO$_3$ ceramics have the highest and lowest gamma attenuation coefficients, respectively. In tab. 4, the average mass attenuation coefficients of (Pb$_{0.9}$Ba$_{0.1}$)ZnO$_3$ over experimental, theoretical and computational values are compared with those of the pure lead.

Given tab. 4, comparing (Pb$_{0.9}$Ba$_{0.1}$)ZnO$_3$ ceramic with pure lead illustrates that at higher energies

**Table 4. Mass attenuation coefficients for some common gamma shields and ceramics studied in this research**

| Energy [keV] | PBZ (A = Zn) | Lead |
|---|---|---|
| 511 | 0.123 | 0.141 |
| 662 | 0.084 | 0.112 |
| 1173 | 0.076 | 0.055 |
| 1332 | 0.058 | 0.0511 |

the mass attenuation coefficient of (Pb$_{0.9}$Ba$_{0.1}$)ZnO$_3$ ceramic is even higher than that of lead. This is because of the presence of other high-*Z* element within the ceramics, which increases the probability of gamma interactions.

**CONCLUSIONS**

In the present work, mass attenuation coefficients of some lead-based ceramics were measured. Moreover, these data were also determined using Monte Carlo MCNP-4C code and compared with theoretical data taken from nuclear library. According to the obtained results, experimental, computational and theoretical data were found to be very close to each other. Moreover, (Pb$_{0.9}$Ba$_{0.1}$)ZnO$_3$ ceramic provided good attenuation properties, which makes it a good choice to be considered as a gamma shield. The promising results of this research show the suitability of using Pb-based ceramic to shield gamma radiation.

148

A. Vejdani-Noghreiyan, *et al.*: Theoretical and Experimental Determination of ...
Nuclear Technology & Radiation Protection: Year 2016, Vol. 31, No. 2, pp. 142-149

## AUTHORS' CONTRIBUTIONS

The samples were prepared by E. Aliakbari and M. Ghasemifard, and gamma spectroscopy was carried out by A. Vejdani-Noghreiyan and E. Aliakbari. Experimental analysis was carried out by A. Ebrahimi-Khankook, A. Vejdani-Noghreiyan and M. Ghasemifard, while the Monte Carlo and theoretical analysis were carried out by A. Ebrahimi-Khankook. The manuscript was written by A. Vejdani-Noghreiyan, A. Ebrahimi-Khankook, and E. Aliakbari. Figures were prepared by E. Aliakbari and M. Ghasemifard.

## REFERENCES

[1] Gurler, O., *et al.*, An Investigation on Determination of Attenuation Coefficients for Gamma-Rays by Monte Carlo Method, *J. Radioanal. Nucl. Chem., 293* (2012), 1, pp. 397-401

[2] Kavanoz, H. B., *et al.*, Photon Parameters for γ-Rays Sensing Properties of Some Thick Oxide Films, *Vacuum., 101* (2014), Mar., pp. 238-245

[3] Bobbio, A., The First Endosseous Alloplastic Implant in the History of Man, *Bull. Hist. Dent., 20* (1972), 1, pp. 1-6

[4] Campbell, P., *et al.*, Biologic and Tribologic Considerations of Alternative Bearing Surfaces, *Clin. Orthop., 418* (2004), Jan., pp. 98-111

[5] Chevalier, J., *et al.*, Ceramics for Medical Applications: A Picture for the Next 20 Years, *J. Eur. Ceram. Soc., 29* (2009), 7, pp. 1245-1255

[6] Celerier, S., *et al.*, Synthesis by Sol-Gel Route of Oxyapatite Powders for Dense Ceramics: Applications as Electrolytes for Solid Oxide Fuel Cells, *J. Eur. Ceram. Soc., 25* (2005), 12, pp. 2665-2668

[7] Krasnyi, B. L., *et al.*, Chemical Resistance of Ceramic Materials in Acids and Alkalis, *Glass. Ceram., 61* (2004), 9-10, pp. 337-339

[8] Medvedovski, E., Alumina-Mullite Ceramics for Structural Applications, *Ceram. Int., 32* (2006), 4, pp. 369-375

[9] Krasnyi, B. L., *et al.*, Chemical Resistance of Ceramic Materials in Acids and Alkalis, *Glass. Ceram., 61* (2004), 9-10, pp. 337-339

[10] She, J. H., *et al.*, Fabrication and Characterization of Highly Porous Mullite Ceramics, *Mater. Chem. Phys., 80* (2003), 3, pp. 610-614

[11] Singh, V. P., *et al.*, Determination of Mass Attenuation Coefficient for Some Polymers Using Monte Carlo Simulation, *Vacuum., 119* (2015), Sep., pp. 284-288

[12] McCaffrey, J. P., *et al.*, Radiation Attenuation by Lead and Nonlead Materials Used in Radiation Shielding Garments, *Med. Phys., 34* (2007), 2, pp. 530-537

[13] El-Sersy, A., *et al.*, Mass Attenuation Coefficients of $B_2O_3$-$Al_2O_3$-$SiO_2$-$CaF_2$ Glass System at 0.662 and 1.25 MeV Gamma Energies, *J. Radioanal. Nucl. Chem., 288* (2010),1, pp. 65-69

[14] Gautam, C., *et al.*, A Review on Infrared Spectroscopy of Borate Glasses with Effects of Different Additives, *Radiat. Meas., 41* (2012), Nov., pp. 84-88

[15] Kaur, U., *et al.*, Comparative Studies of Different Concretes on the Basis of Some Photon Interaction Parameters, *Appl. Radiat. Isotopes., 70* (2012), 1, pp. 233-240

[16] ***, Appendix C: Electron Binding Energies (eV), Physics for Radiation Protection: A Handbook, 2nd edn, John Wiley & Sons, New York, 2006

[17] Colorado, H. A., *et al.*, Wollastonite Based-Chemically Bonded Phosphate Ceramics with Lead Oxide Contents under Gamma Irradiation, *J. Nucl. Mater., 425* (2012), 1, pp. 197-204

[18] Akkurt, I., *et al.*, Radiation Shielding of Concretes Containing Different Aggregates. *Cement, Concrete. Comp., 28* (2006), 2, pp. 153-157

[19] Cevik, U., *et al.*, Determination of Attenuation Coefficients, Thicknesses and Effective Atomic Numbers for $CuInSe_2$ Semiconductor, *Nucl. Instrum. Meth. B., 247* (2006), 2, pp. 173-179

[20] Turkmen, I., *et al.*, Calculation of Radiation Attenuation Coefficients in Portland Cements Mixed with Silica Fume, Blast Furnace Slag and Natural Zeolite, *Ann. Nucl. Energy., 35* (2008), 10, pp. 1937-1943

[21] Han, I., *et al.*, Mass Attenuation Coefficients, Effective Atomic and Electron Numbers of Ti and Ni Alloys, *Radiat. Meas., 44* (2009), 3, pp. 289-294

[22] Akkurt, I., *et al.*, The Boronizing Effect on the Radiation Shielding and Magnetization Properties of AISI 316L Austenitic Stainless Steel, *Nucl. Eng. Des., 241* (2011), 1, pp. 55-58

[23] Akkurt, I., *et al.*, Photon Attenuation Coefficients of Concrete Including Marble Aggregates, *Ann. Nucl. Energy, 43* (2012), May, pp. 56-60

[24] Kucuk, N., *et al.*, Mass Attenuation Coefficients, Effective Atomic Numbers and Effective Electron Densities for Some Polymers, *Radiat. Prot. Dosim., ncs 091* (2012)

[25] Limkitjaroenporn, P., *et al.*, Physical, Optical, Structural and Gamma-Ray Shielding Properties of Lead Sodium Borate Glasses, *J. Phys. Chem. Solids., 72* (2011), 4, pp. 245-251

[26] Jackson, D. F., *et al.*, X-Ray Attenuation Coefficients of Elements and Mixtures, *Phys. Rep., 70* (1981), 3, pp. 169-233

[27] Ghasemifard, M., *et al.*, Microstructural and Optical Characterization of PZT Nanopowder Ceramic Prepared at Low Temperature, *Physica. E., 41* (2009), 3, pp. 418-422

[28] Ghasemifard, M., *et al.*, Synthesis and Structure of PMN-PT Ceramic Nanopowder Free from Pyrochlore Phase, *Ceram. Int., 35* (2009), 7, pp. 2899-2905

[29] El-Khayatt, A. M., *et al.*, Photon Attenuation Coefficients of Heavy-Metal Oxide Glasses by MCNP Code, XCOM Program and Experimental Data: a comparison Study, *Nucl. Inst. Meth. Phy. Research A., 735* (2013), Jan., pp. 207-212

[30] Sharifi, S. H., *et al.*, Comparison of Shielding Properties for Ordinary, Barite, Serpentine and Steel-Magnetite Concretes Using MCNP-4C Code and Available Experimental Results, *Ann. Nuc. Energy., 53* (2013), Mar., pp. 529-534

[31] Shirmardi, S. P., *et al.*, Comparison of Photon Attenuation Coefficients of Various Barite Concretes and Lead by MCNP Code, XCOM and Experimental Data, *Ann. Nucl. Energy, 55* (2013), May, pp. 288-291

[32] Singh, V. P., *et al.*, Monte Carlo Simulation of Gamma Rayshielding Parameters of Concretes, *Nucl. Eng. Des., 265* (2013), Dec., pp. 1071-1077

[33] Briesmeister, J. F., MCNPTM-A General Monte Carlo N-Particle Transport Code Version 4C. RSICC Computer Code Collection, ccc700, Oak Ridge National Laboratory, Oak Ridge, Tenn., USA, 2000

[34] Bartesaghi, G., *et al.*, Evaluation of all Dose Components in the LVR-15 Reactor Epithermal Neutron Beam Using Fricke Gel Dosimeter Layers, *Appl. Radiat. Isotopes., 67* (2009), 7, pp. S199-S201

[35] Singh, V. P. *et al.*, Investigation on Radiation Shielding Parameters of Ordinary, Heavy and Super Heavy Concretes, *Nucl Technol Radiat, 29* (2014) 2, pp. 149-156

[36] Demir, N., *et al*., Investigation of Mass Attenuation Coefficients of Water, Concrete and Bakelite at Different Energies Using the FLUKA Monte Carlo code, *J. Radioanal. Nucl. Chem., 298* (2013), 2, pp. 1303-1307

[37] Marinković, P., Study of Influence of Buildup Factor form on Simulated Radiographic Image, *Nucl Technol Radiat, 2*4 (2009), 1, pp. 38-45

[38] Sogut, O., *et al*., Chemical Effects on K /K  X-Ray Intensity Ratios of Mo, Ag, Cd, Ba, La, Ce Compounds and Total Mass Attenuation Coefficients of Fe and Cu, *Spectrochim. Acta. B., 56* (2001), 8, pp. 1367-1374

[39] Icelli, O., *et al*., Measurement of Mass Attenuation Coefficients of Some Boron Compounds and the Trommel Sieve Waste in the Energy Range

15.746-40.930 keV, *J. Quant. Spectrosc. Ra., 78* (2003), 2, pp. 203-210

[40] Icelli, O., *et al*., The Mass Attenuation Coefficients in Some Vanadium and Nickel Compounds, *J. Quant. Spectrosc. Ra., 88* (2004), 4, pp. 519-524

[41] ***, Radiation Spectroscopy with Scintillators. in: *Radiation Detection and Measurement,* 3rd ed., John Wiley & Sons, New York, 2010

**Алиреза ВЕЈДАНИ-НОГРЕИЈАН, Елхам АЛИАКБАРИ,
Атијех ЕБРАХИМИ-КАНКУК, Махди ГАЗЕМИФАРД**

## ТЕОРИЈСКО И ЕКСПЕРИМЕНТАЛНО ОДРЕЂИВАЊЕ МАСЕНИХ АТЕНУАЦИОНИХ КОЕФИЦИЈЕНАТА КЕРАМИКА НА БАЗИ ОЛОВА И ЊИХОВО ПОРЕЂЕЊЕ СА СИМУЛАЦИЈОМ

Извршено је поређење масених атенуационих коефицијената керамика на бази олова одређених експерименталним путем са вредностима добијеним теоријским моделом и Монте Карло симулацијом. Керамике на бази олова припреманe су методом мешаног оксида, а процена кристалне структуре ручно направљених керамика обављена је дифракционом анализом X-зрачења. Експериментални резултати добро се слажу са теоријским вредностима и вредностима добијеним симулацијом. Међутим, за две вредности енергија гама зрачења, уочене су мале разлике између експерименталних и теоријских резултата. Додавањем адитива керамици и посматрањем промена у заштитним особинама као што је флексибилност, могу се синтетизовати и оптимизовати керамике погодне за заштиту од неутрона.

*Кључне речи: атенуациони коефицијент, CsI(Tl) детектор, керамика на бази олова, MCNP-4C*